

The Jackson Laboratory

The Mouseion at the JAXlibrary

Faculty Research 2024

Faculty & Staff Research

2-1-2024

Transcriptional and functional consequences of Oncostatin M signaling on young Dnmt3a-mutant hematopoietic stem cells.

Logan S Schwartz

Kira Young

Timothy M Stearns

Nathan Boyer

Kristina D Mujica

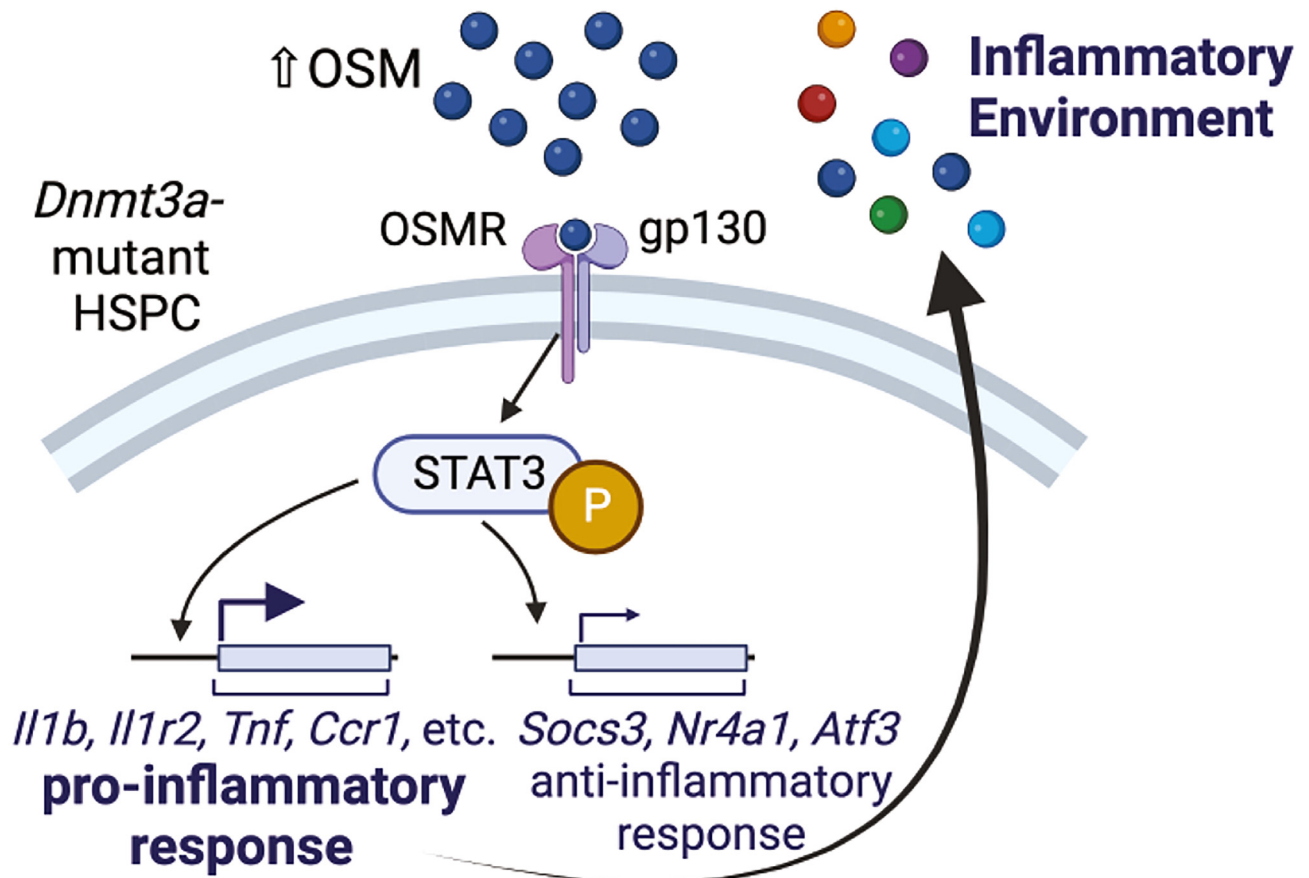
See next page for additional authors

Follow this and additional works at: <https://mouseion.jax.org/stfb2024>

Authors

Logan S Schwartz, Kira Young, Timothy M Stearns, Nathan Boyer, Kristina D Mujica, and Jennifer J. Trowbridge

Transcriptional and functional consequences of Oncostatin M signaling on young *Dnmt3a*-mutant hematopoietic stem cells





Transcriptional and functional consequences of Oncostatin M signaling on young *Dnmt3a*-mutant hematopoietic stem cells

Logan S. Schwartz^{a,b}, Kira A. Young^a, Timothy M. Stearns^a, Nathan Boyer^a, Kristina D. Mujica^a, and Jennifer J. Trowbridge^{a,b*}

^aThe Jackson Laboratory, Bar Harbor, ME; ^bSchool of Graduate Biomedical Sciences, Tufts University School of Medicine, Boston, MA

Age-associated clonal hematopoiesis (CH) occurs due to somatic mutations accrued in hematopoietic stem cells (HSCs) that confer a selective growth advantage in the context of aging. The mechanisms by which CH-mutant HSCs gain this advantage with aging are not comprehensively understood. Using unbiased transcriptomic approaches, we identified Oncostatin M (OSM) signaling as a candidate contributor to age-related *Dnmt3a*-mutant CH. We found that *Dnmt3a*-mutant HSCs from young adult mice (3–6 months old) subjected to acute OSM stimulation do not demonstrate altered proliferation, apoptosis, hematopoietic engraftment, or myeloid differentiation. *Dnmt3a*-mutant HSCs from young mice do transcriptionally upregulate an inflammatory cytokine network in response to acute in vitro OSM stimulation as evidenced by significant upregulation of the genes encoding IL-6, IL-1 β , and TNF α . OSM-stimulated *Dnmt3a*-mutant HSCs also demonstrate upregulation of the anti-inflammatory genes *Socs3*, *Atf3*, and *Nr4a1*. In the context of an aged bone marrow (BM) microenvironment, *Dnmt3a*-mutant HSCs upregulate proinflammatory genes but not the anti-inflammatory genes *Socs3*, *Atf3*, and *Nr4a1*. The results from our studies suggest that aging may exhaust the regulatory mechanisms that HSCs employ to resolve inflammatory states in response to factors such as OSM. © 2024 ISEH – Society for Hematology and Stem Cells. Published by Elsevier Inc. This is an open access article under the CC BY-NC-ND license (<http://creativecommons.org/licenses/by-nc-nd/4.0/>)

HIGHLIGHTS

- Oncostatin M (OSM) signaling is elevated in *Dnmt3a*-mutant hematopoietic stem cells (HSCs) with aging.
- OSM does not functionally impact young *Dnmt3a*-mutant HSCs.
- OSM activates both pro- and anti-inflammatory genes in young *Dnmt3a*-mutant HSCs.
- In aging, *Dnmt3a*-mutant HSCs elevate pro- but not anti-inflammatory genes.

The process of aging has a profound impact on tissues and cells throughout the body. In the hematopoietic stem and progenitor cell (HSPC) compartment, aging is accompanied by the acquisition of somatic mutations. Given the long-lived nature of the HSPC pool, these mutations can be propagated for many cellular generations and through most mature hematopoietic cell progeny. Although most of these somatic mutations are considered neutral, a subset can confer a selective growth advantage to HSPCs, leading to a condition termed age-associated clonal hematopoiesis (CH). The most common CH mutations are found in a subset of genes that encode canonical epigenetic or chromatin regulatory proteins, such as DNA

methyltransferase 3A (DNMT3A), tet methylcytosine dioxygenase 2 (TET2) and additional sex combs like-1 (ASXL1) [1,2]. Although CH is not a disease *per se*, it is associated with increased risk of age-associated pathologies, such as blood cancers and ischemic stroke [1–7]. Understanding the cellular and molecular mechanisms underlying the selective advantage of HSPCs harboring somatic mutations and how and in whom this is a risk factor for age-associated disease will further inform our understanding of CH-associated conditions.

By creating and utilizing genetically engineered mouse models, many research groups have reported the functional and molecular consequences of the most common human CH-associated mutations in *DNMT3A*, *TET2*, and *ASXL1* [1,2,7–9]. In some of these studies, chronic stress and inflammation were found to act as selective pressures contributing to expansion of CH and development of CH-associated pathologies [1,10,11]. CH-mutant HSCs have different molecular and functional responses to proinflammatory cytokine signaling [12,13], and recent work suggests that CH-mutant hematopoietic cells can induce and maintain a proinflammatory state [14]. For example, *Dnmt3a*-mutant hematopoiesis is associated with elevated levels of IFN γ [15,16], IL-6 [17] and TNF α [18]. *Tet2*-mutant hematopoiesis is associated with elevated levels of IL-6 [19], IL-8 [20], IL-1 β [21–23] and TNF α [24]. *Asx1*-mutant CH is associated with increased IFN γ and TNF α [25]. The extent to which multiple

Address correspondence to Jennifer J. Trowbridge, The Jackson Laboratory, 600 Main Street, Bar Harbor, ME 04609, USA; E-mail: Jennifer.trowbridge@jax.org

0301-472X/© 2024 ISEH – Society for Hematology and Stem Cells. Published by Elsevier Inc. This is an open access article under the CC BY-NC-ND license (<http://creativecommons.org/licenses/by-nc-nd/4.0/>)

<https://doi.org/10.1016/j.exphem.2023.11.005>

cytokines activate the same underlying inflammatory network contributing to CH and CH-associated pathologies and whether individual cytokines have context-dependent effects remains unknown. Addressing this gap in knowledge is important when considering therapeutic interventions that will be most effective in individuals at risk of CH-associated pathologies.

Using a Cre-inducible mouse model that we previously engineered to express a specific *Dnmt3a* mutation associated with CH and acute myeloid leukemia (*Dnmt3a*^{R878H}) [26], we found that placing *Dnmt3a*-mutant HSPCs in a middle-aged bone marrow (BM) microenvironment in the context of elevated proinflammatory cytokines promoted their selective advantage [18]. We discovered that TNF α :TNFR1 signaling was a key mediator of the selective advantage of *Dnmt3a*-mutant HSCs in the context of a middle-aged BM microenvironment [18]. However, as described above, TNF α is not the only cytokine known to contribute to *Dnmt3a*-mutant CH. Here, we report on our findings investigating Oncostatin M (OSM) as a proinflammatory cytokine associated with CH in *Dnmt3a*-mutant mice.

METHODS

Animals

C57BL/6J (JAX:000664) and B6.SJL-*PtprcaPepcb*/BoyJ [27] (JAX:002014, referred to as CD45.1⁺) mice were obtained from and aged within The Jackson Laboratory. *Dnmt3a*^{fl-R878H/+} mice (JAX:032289) were crossed to B6.Cg-Tg(Mx1-cre)1Cgn/J mice (JAX:003556, referred to as Mx-Cre). In all experiments, control (+/+) mice carried a single copy of the Mx-Cre allele. The Jackson Laboratory's Institutional Animal Care and Use Committee approved all experiments. To induce Mx-Cre, mice were intraperitoneally injected once every other day for five total injections with 15 mg/kg high-molecular-weight polyinosinic-polycytidylic acid (polyI:C) (InvivoGen). In all experiments, mice were used >4 weeks following polyI:C administration.

Peripheral Blood Analysis

Blood was collected from mice via the retro-orbital sinus, and red blood cells were lysed before staining with the following fluorochrome-conjugated antibodies: BV650 CD45.1 (BioLegend clone A20), AlexaFluor700 CD45.2 (BioLegend clone 104), BUV496 B220 (BD Biosciences clone RA3-6B2), PerCP-Cy5.5 CD3e (BioLegend clone 145-2C11), APC-Cy7 CD11b (BioLegend clone M1/70), APC Ly6g (BioLegend clone 1A8), BV605 Ly6c (BioLegend clone HK1.4), BV421 Ter-119 (BioLegend clone TER-119), and PE-Cy7 F4/80 (Invitrogen BM8). Data were collected using a LSRII (BD Biosciences) and analyzed using FlowJo V10 (BD Biosciences).

Isolation and Phenotyping of Hematopoietic Stem and Progenitor Cells

BM cells were isolated from pooled and crushed femurs, tibiae, iliac crests, sternums, forepaws, and spinal columns of individual mice. BM mononuclear cells (MNCs) were isolated by Ficoll-Paque (GE Healthcare Life Sciences) density centrifugation or IX RBC Lysis Buffer (eBioscience) and stained with a combination of fluorochrome-conjugated antibodies: c-Kit (BD Biosciences, BioLegend clone 2B8), Sca-1 (BioLegend clone D7), CD150 (BioLegend clone

TC15-12F12.2), CD48 (BioLegend clone HM48-1), CD34 (BD Biosciences clone RAM34), FLT3 (BioLegend clone A2F10), CD11b (BioLegend clone M1/70), mature lineage (Lin) marker mix (B220 (BD Biosciences, BioLegend clone RA3-6B2), CD4 (BioLegend clone RM4-5), CD5 (BioLegend clone 53-7.3), CD8a (Biosciences, BioLegend clone 53-6.7), Ter-119 (BioLegend clone TER-119), and Gr-1 (BioLegend, Invitrogen clone RB6-8C5), and the viability stain propidium iodide (PI) or 4',6-diamidino-2-phenylindole (DAPI). For transplants, CD45.1 (BioLegend clone A20) and CD45.2 (BioLegend clone 104) antibodies were used to distinguish genotypes of donor and recipient mice. The following cell surface markers were used to isolate or phenotype the following cell types: hematopoietic stem cells (HSCs), Lin⁻ Sca-1⁺ c-Kit⁺ Flt3⁻ CD150⁺ CD48⁻; HSPCs, Lin⁻ Sca-1⁺ c-Kit⁺; granulocyte/macrophage-primed multipotent progenitors (MPP^{G/M}), Lin⁻ Sca-1⁺ c-Kit⁺ Flt3⁻ CD150⁻ CD48⁺; common myeloid progenitor cells (CMPs) Lin⁻ Sca-1⁻ c-Kit⁺ CD34⁺ Fc γ R⁻; and granulocyte-macrophage progenitors (GMPs), Lin⁻ Sca-1⁻ c-Kit⁺ CD34⁺ Fc γ R⁺. Data were collected using a BD FACSymphony A5 or cells were prospectively isolated using a FACSymphony S6 (BD Biosciences). All flow cytometry data were analyzed using FlowJo V10.

Cell Cycle Analysis

Briefly, 5,000 HSPCs were sorted directly into tissue culture-treated 96-well plates (Falcon) containing StemSpan Serum-Free Expansion Medium II (SFEM II; STEMCELL Technologies) with penicillin and streptomycin (Pen-Strep, Fisher Scientific) and stem cell factor (SCF, 100 ng/mL, BioLegend), thrombopoietin (TPO, 50 ng/ μ L, Pepro-Tech), with or without OSM (500 ng/mL, BioLegend) for 24 hours at 37°C and 5% CO₂. Cells were stained with Ghost UV450 viability dye (Cytek Biosciences) and fixed with the FIX & PERM Cell Permeabilization Kit (Invitrogen) following the manufacturer's protocol. Following fixation, cells were stained with FITC anti-mouse/human Ki-67 (BioLegend) and DAPI. Data were collected on a BD FACSymphony A5.

Apoptosis Analysis

Briefly, 5,000 HSPCs were sorted directly into 96-well plates containing SFEM II with Pen-Strep and SCF (100 ng/mL), TPO (50 ng/ μ L), and with or without OSM (500 ng/mL) for 24 hours at 37°C and 5% CO₂. Cells were stained with Annexin V and PI using the Annexin A5 Apoptosis Detection Kit (BioLegend). Data were collected on a FACSymphony A5 (BD Biosciences).

Colony-Forming Unit (CFU) Assay

HSCs or HSPCs were isolated and plated in MethoCult GF M3434 (STEMCELL Technologies) with or without OSM (500 ng/mL) and cultured at 37°C and 5% CO₂. Colonies were scored between 6- and 14-days postplating using a Nikon Eclipse TS100 inverted microscope. For serial replating, cells were harvested by washing the plates, and 10,000 cells (from HSCs) or 15,000 cells (from HSPCs) were replated into fresh MethoCult GF M3434 with or without OSM (500 ng/mL).

In Vitro Culture with Cytokine-Rich and Cytokine-Poor Media

We followed a published protocol to generate cytokine-rich and cytokine-poor media [28]. Briefly, 500 cells were sorted directly into 96-

well plates in 200 μ L of Iscove's Modified Dulbecco's Medium (IMDM) containing 5% fetal bovine serum (FBS), 50 U/mL penicillin, 50 μ g/mL streptomycin, 2 mM L-glutamine, 0.1 mM nonessential amino acids, 1 mM sodium pyruvate, and 50 μ M 2-mercaptoethanol. For cytokine-rich media, the medium was supplemented with SCF (25 ng/mL), TPO (25 ng/mL), Flt3L (25 ng/mL), IL-11 (25 ng/mL), IL-3 (10 ng/mL), granulocyte-macrophage colony-stimulating factor (GM-CSF, 10 ng/mL) and EPO (4 U/mL) (all from PeproTech). For cytokine-poor media, this was supplemented with SCF (25 ng/mL) and G-CSF (25 ng/mL, PeproTech). Phosphate-buffered saline (PBS) or OSM was added at 500 ng/mL to both media. After 48 hours of culture at 37°C and 5% CO₂, cells were harvested. DAPI was used to determine live cells, and data were collected on a FACSymphony A5.

Polyvinyl Alcohol (PVA) Culture and In Vivo Transplantation

For the noncompetitive PVA culture and transplant experiment, 50 CD45.2⁺ HSCs were sorted into a 96-well plate with Ham's F12 media containing 1X penicillin/streptomycin/glutamine (Gibco), 10 mmol/L HEPES (Gibco), 1X insulin/transferrin/selenium/ethanolamine (Gibco), 100 ng/mL rmTPO (BioLegend), 10 ng/mL rmSCF (STEMCELL Technologies), and 1 mg/mL polyvinyl alcohol (Sigma) with or without 500 ng/mL rmOSM and cultured for 7 days at 37°C and 5% CO₂, as previously described [29]. Then, 500 ng/mL OSM or vehicle was added to the cultures on days 4 and 6. On day 7, the wells were harvested, mixed with 10⁶ CD45.1⁺ BM MNCs, and transplanted into young, lethally irradiated (12 Gy gamma irradiation, split dose) CD45.1⁺ recipients. Peripheral blood (PB) and BM data were collected at 6 months after transplant using a BD LSR II instrument.

For competitive PVA culture and transplant experiments, 25 CD45.2⁺ HSCs from control or R878H/+ donors (CD45.2⁺) and 25 CD45.1⁺CD45.2⁺ HSCs from wild-type F1 mice were sorted into a 96-well plate with Ham's F12 media containing 1X penicillin/streptomycin/glutamine (Gibco), 10 mmol/L HEPES (Gibco), 1X insulin/transferrin/selenium/ethanolamine (Gibco), 100 ng/mL rmTPO (BioLegend), 10 ng/mL rmSCF (STEMCELL Technologies) and 1mg/mL PVA (Sigma) with or without 500 ng/mL rmOSM and cultured for 7 days at 37°C and 5% CO₂, as previously described [29]. Briefly, 500 ng/mL rmOSM or vehicle was added to the cultures on days 4 and 6. On day 7, the wells were harvested, mixed with 10⁶ CD45.1⁺ BM MNCs, and transplanted into young, lethally irradiated (12 Gy gamma irradiation, split dose) CD45.1⁺ recipients. PB and BM were collected at 6 months after transplant using a BD LSR II instrument.

Fluorescent OSM Binding

Briefly, 100 μ g rmOSM (BioLegend) was concentrated by centrifugation (Amicon Ultra-0.5 Centrifugal Filter Unit) and fluorescently labeled using the AlexaFluor 488 Antibody Labeling Kit following the manufacturer's protocol. Briefly, 10⁷ WBM cells were treated with FC block then stained for 30 min with PBS or fluorescently labeled rmOSM at 37°C for 30 min. After 30 min, cells were stained with an antibody cocktail for the identification of HSCs and HSPCs as detailed above. Cells were washed and assessed on a BD FACSymphony A5 SE. As positive control, a single cell suspension of liver cells was prepared using the Miltenyi Liver Kit (MiltenyiBiotec).

Phospho-Flow Cytometry

Briefly, 1000 LSK cells were sorted into StemSpan SFEM II media (STEMCELL Technologies). Cells were pelleted and resuspended in StemSpan SFEM II with or without 500 ng/mL rmOSM and incubated at 37°C for 20, 60 or 80 min. Cells were then fixed using 16% paraformaldehyde for 10 min at room temperature followed by ice-cold acetone for 10 min. Cells were then pelleted, washed and stained with AlexaFluor 488 Mouse Anti-Stat3 (Tyr705) (D3A7) XP Rabbit mAb (Cell Signaling Technologies) or PE-Cy7 Mouse Anti-Stat5 (pY694) (BD) for 30 min at room temperature before data collection using a BD FACSymphony A5 SE.

RNA Sequencing

Briefly, 2,000 HSCs were sorted into StemSpan SFEM II media with TPO (50 ng/mL) and SCF (100 ng/mL). PBS or OSM (500 ng/mL) was added to each well and incubated at 37°C for 60 min. Total RNA was isolated from flash-frozen pellets using the RNeasy Micro Kit (Qiagen) including the optional DNase digest step. RNA concentration and quality were assessed using the RNA 6000 Pico Assay (Agilent Technologies). Libraries were constructed using the SMARTer Stranded Total RNA-Seq Kit v2-Pico (Takara), according to the manufacturer's protocol. Library concentration and quality were assessed using the D5000 ScreenTape (Agilent Technologies) and Qubit dsDNA HS Assay (ThermoFisher). Libraries were subject to 75 bp paired-end sequencing on an Illumina NextSeq 500 using the High Output Reagent Kit v2.5 or 150 bp paired-end sequencing on an Illumina NovaSeq 6000 using the S4 Reagent Kit v1.5 both at a sequencing depth of >35 million reads per sample. Trimmed alignment files were processed using RSEM (v1.3.3). Alignment was completed using Bowtie 2 (v2.4.1). Expected read counts per gene produced by RSEM were rounded to integer values, filtered to include only genes that had at least two samples within a sample group having a counts per million reads > 1, and passed to R (v4.1.3) and edgeR (v3.36.0) for differential expression analysis. A negative binomial generalized log-linear model was fit to the read counts for each gene. The dispersion trend was estimated by Cox-Reid approximate profile likelihood followed by empirical Bayes estimate of the negative binomial dispersion parameter for each tag, with expression levels specified by a log-linear model. Likelihood ratio tests for coefficient contrasts in the linear model were evaluated producing a *p* value per contrast. The Benjamini and Hochberg's algorithm (*p* value adjustment) was used to control the false discovery rate. Differentially expressed genes were investigated for overlap with published datasets using Gene Set Enrichment Analysis, and upstream regulators were predicted using Ingenuity Pathway Analysis software. Features with fold change (FC) > 1.5 or < -1.5 and *p* < 0.05 were declared significantly differentially expressed.

Socs3 mRNA Expression Assays

For *Socs3* expression assays, HSPCs were sorted into 750 μ L of StemSpan SFEM II with vehicle or 500 ng/mL OSM and incubated at 37°C for 20, 40, 60, or 80 min. Following each incubation, actinomycin D (Sigma) was added, and cells were incubated for an additional 20 min at 37°C. Samples were pelleted and flash frozen. For *Socs3* stability assays, HSPCs were sorted into 750 μ L of StemSpan SFEM II with vehicle or 500 ng/mL OSM and incubated at 37°C for 60 min. Actinomycin D was added for 20, 40, 60, or 80 min at 37°C

C. Samples were pelleted and flash frozen. From all samples, RNA was isolated using the RNeasy Micro Kit (Qiagen), and cDNA was made using the qPCR Bio cDNA Synthesis Kit (PCR Biosystems). Quantitative PCR was performed using Power SYBR on the QuantStudio 7 Real-Time PCR System (ThermoFisher Scientific). mRNA expression levels were calculated relative to the housekeeping gene, *B2m*.

Enzyme-Linked Immunoassay (ELISA)

BM fluid was collected from 3-, 14-, and 22-month-old C57BL/6J mice by needle flushing of femurs with 200 μ L PBS. The OSM concentration was determined using the Quantikine ELISA for mouse Oncostatin M (R&D Systems) using a Spectramax i3 (Molecular Devices) plate reader.

Statistical Analysis

All statistical tests including evaluation of the normal distribution of data and examination of variance between groups were performed using Prism 9 software (GraphPad). Figure 6C was created using BioRender.com licensed to The Jackson Laboratory.

Data Availability

Raw RNA-seq data are available at the Gene Expression Omnibus under accession number GSE236693.

RESULTS

Dnmt3a-Mutant HSCs Activate Oncostatin M Signaling in an Aged BM Microenvironment

Our previously published work profiled molecular signatures associated with *Dnmt3a*-mutant (R878H/+) hematopoiesis in a middle-aged BM microenvironment by performing RNA sequencing (RNA-seq) on independent biological replicates of control and *Dnmt3a*-mutant HSCs re-isolated from young and middle-aged recipient mice (Figure 1A) [18]. In new analysis of these data, enrichment of a hallmark inflammatory response signature was observed in *Dnmt3a*-mutant HSCs compared with control HSCs in middle-aged recipient mice but not in young recipient mice (Figure 1B), suggesting that a middle-aged environment promotes transcriptional responses to inflammatory factors in *Dnmt3a*-mutant HSCs. Examining the top leading edge genes using gene set enrichment analysis, increased expression of the IFN γ -regulated genes *Bst2*, *Klf6*, and *Icam1*; the inflammatory-responsive receptors *Tlr2* and *Ccr12*; and the copper transporter *Slc31a2* was observed. *Osm* was the only leading edge gene encoding a secreted molecule, Oncostatin M, which is an IL-6 family cytokine known to be involved in the immunopathogenesis of solid tumors and myeloma [30–34]. Given this observation, we hypothesized that increased expression of *Osm* results in a feed-forward activation loop of the OSM signaling pathway.

To test this hypothesis, we interrogated the expression of a subset of genes known to be involved in and/or regulated by OSM signaling including transcripts encoding OSM signaling receptors (*Osmr*, *Il6st*), downstream kinases and signaling molecules (e.g., *Shc1*, *Mapk14*, *Prkcb*, *Nfkb1*), and transcription factor targets (e.g., *Egr1*, *Fos*, *Junb*, *Jund*). We observed trends toward increased expression and significant increase in expression ($p < 0.05$) in most genes examined in *Dnmt3a*-mutant HSCs compared with control HSCs in middle-aged

recipient mice but not in young recipient mice (Figure 1C). We used the upstream regulator analysis feature of ingenuity pathway analysis as a complementary approach to examine activation of OSM signaling in *Dnmt3a*-mutant HSCs compared with control HSCs in middle-aged recipient mice. Activation of an OSM-driven IL-6:STAT3 module was observed in *Dnmt3a*-mutant HSCs in middle-aged recipient mice (Figure 1D). These results are consistent with activation of OSM signaling in *Dnmt3a*-mutant HSCs in the specific context of a middle-aged environment.

Acute OSM Stimulation Does Not Impact Cell Cycle, Apoptosis, Proliferation, or Myeloid Differentiation of Young *Dnmt3a*-Mutant HSPCs

Given that activation of OSM signaling is associated with expanded *Dnmt3a*-mutant hematopoiesis in an aged BM microenvironment, we hypothesized that OSM as a single stimulus would be sufficient to promote the selective advantage of young *Dnmt3a*-mutant HSPCs. To test the effect of recombinant OSM on young *Dnmt3a*-mutant HSPC cycling, cell cycle status was evaluated using Ki-67 and DAPI staining. Control and *Dnmt3a*-mutant HSPCs were prospectively isolated from young adult mice (3–6 months old) and stimulated overnight with 0, 100 or 500 ng/mL recombinant murine OSM. Following flow cytometry analysis, cells were gated into G0 (Ki-67- DAPI-), G1 (Ki-67+ DAPI-) and S/G2/M (Ki-67+ DAPI+) fractions. No significant differences were observed in these proportions across any of the conditions, although there was a trend toward increased S/G2/M in *Dnmt3a*-mutant HSPCs with increasing doses of OSM (Figure 2A). To test the effect of recombinant OSM on young *Dnmt3a*-mutant HSPC survival, apoptosis was assessed using Annexin V and propidium iodide (PI) staining. Control and *Dnmt3a*-mutant HSPCs were prepared and stimulated overnight as detailed above. Following flow cytometry analysis, cells were gated into live (Annexin V- PI-), early apoptotic (Annexin V + PI-), late apoptotic (Annexin V + PI+), and necrotic (Annexin V- PI +) fractions. No significant differences in these proportions were observed across any of the conditions (Figure 2B). Together, these data suggest that young control and *Dnmt3a*-mutant HSPCs do not respond to acute OSM stimulation with respect to altered cell cycle and apoptosis parameters.

To test the effect of recombinant OSM on myeloid differentiation potential, control and *Dnmt3a*-mutant HSPCs were prospectively isolated from young adult mice and plated into myeloid methylcellulose media to quantify CFU. The myeloid methylcellulose media was supplemented with 0, 100, or 500 ng/mL recombinant murine OSM. After 7 days of culture, no differences in CFU formation were observed across any of the conditions (Figure 2C). This result suggests that control and *Dnmt3a*-mutant HSPCs do not respond to OSM by altering their myeloid differentiation potential. To examine CFU replating potential, control and *Dnmt3a*-mutant HSPCs as well as HSCs with 0 or 500 ng/mL recombinant murine OSM continued to be passaged. As expected, increased CFU replating potential from *Dnmt3a*-mutant versus control HSPCs and HSCs was observed (Figure 2D). However, there was no observed effect of OSM on either control or *Dnmt3a*-mutant CFU replating capacity.

A limitation of the above CFU studies is that the effect of OSM is being evaluated in the presence of a full complement of cytokines that drive robust myeloid/erythroid cell differentiation (SCF, IL-3, IL-6, and EPO). To examine the effects of OSM on HSPC proliferation in conditions replicating stress, 0 or 500 ng/mL recombinant murine

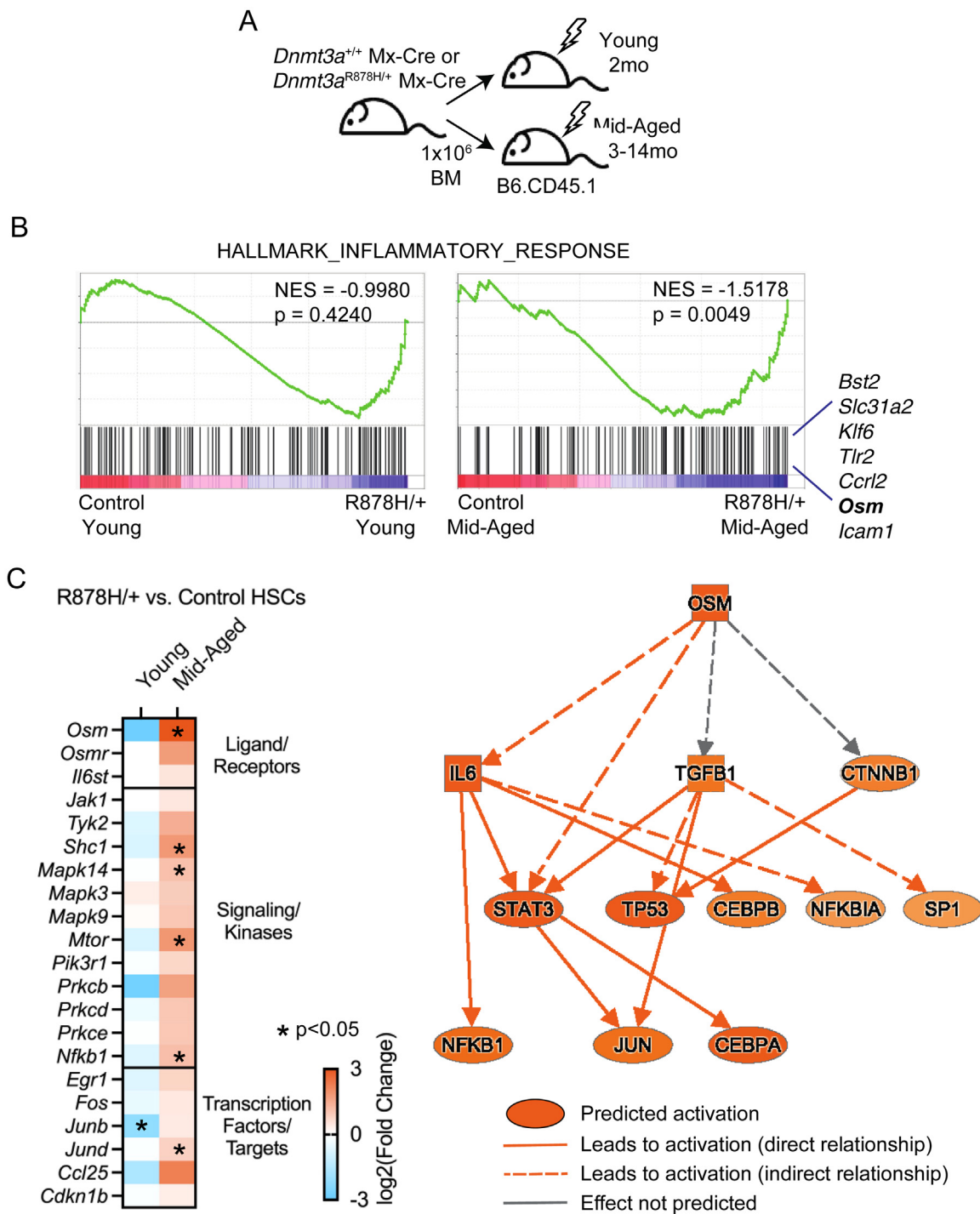


Figure 1 *Dnmt3a*-mutant HSCs upregulate *Osm* and OSM signaling genes in a middle-aged BM environment. **(A)** Schematic of transplant design into young (2 month) and middle-aged (13–14 months) recipient mice. HSCs ($Lin^- c\text{-Kit}^+ Sca\text{-}1^+ Flt3^- CD150^+ CD48^-$) were isolated at 4 months post-transplant and used for RNA-sequencing [18]. $n = 3\text{--}4$ biological replicates. **(B)** Gene set enrichment analysis of a hallmark inflammatory response signature in control vs. *Dnmt3a*-mutant (R878H/+) HSCs in young recipient mice (left) and in middle-aged recipient mice (right). **(C)** Heatmap of $\log_2(FC)$ expression in OSM signaling pathway genes in *Dnmt3a*-mutant (R878H/+) compared with control HSCs in young (left column) and middle-aged (right column) recipient mice. * $p < 0.05$. **(D)** Ingenuity pathway analysis showing predicted activation of OSM signaling in *Dnmt3a*-mutant (R878H/+) vs. control HSCs in middle-aged recipient mice. BM=Bone marrow; HSCs=hematopoietic stem cells; HSPCs=hematopoietic stem and progenitor cells; FC=fold change; OSM=Oncostatin M.

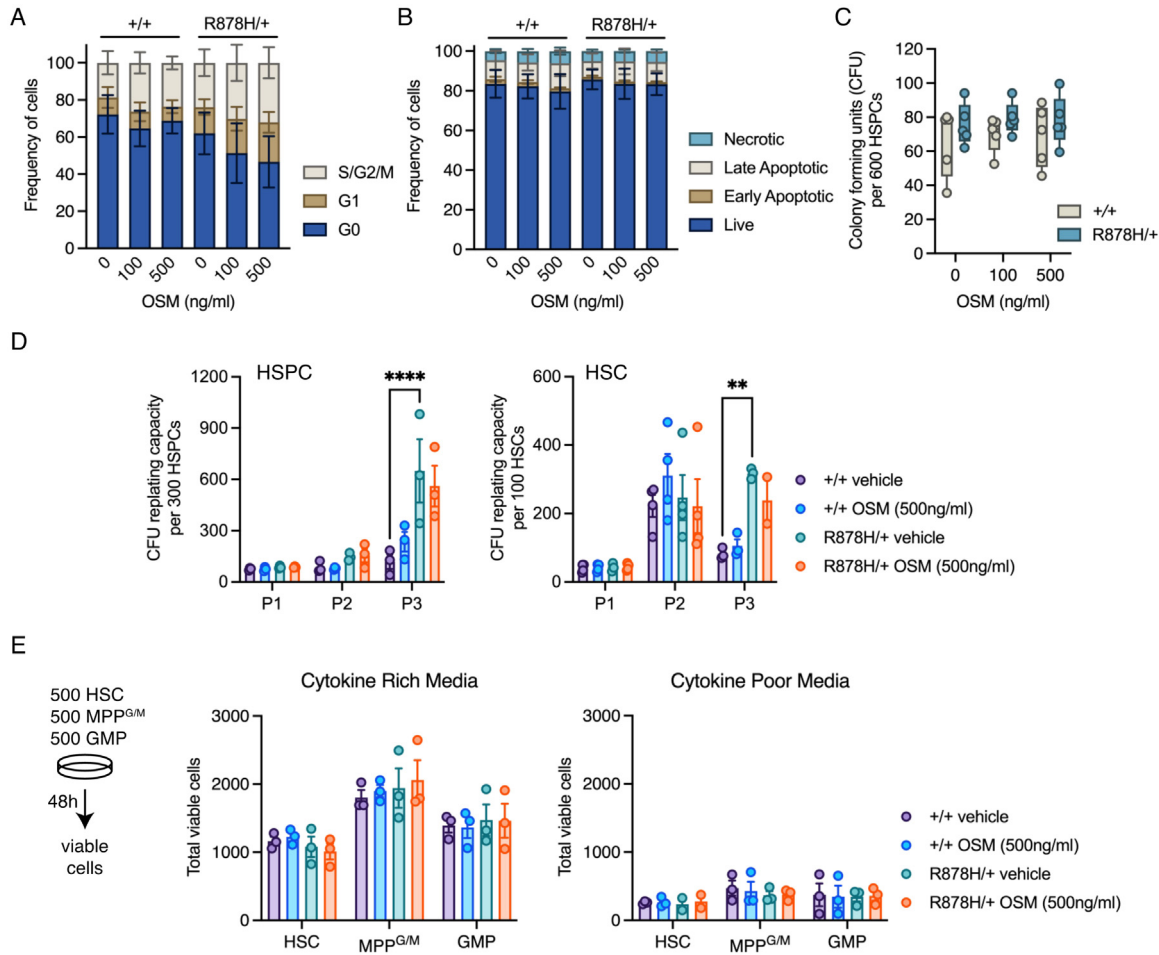


Figure 2 Cell cycle, apoptosis, proliferation, and myeloid differentiation in young *Dnmt3a*-mutant HSPCs are unaltered by acute OSM stimulation.

(A) Frequency of control (+/+) and *Dnmt3a*-mutant (R878H/+) HSPCs in G0, G1, and S/G2/M cell cycle phases after stimulation with 0, 100, or 500 ng/mL OSM for 24 hours. Bars represent mean \pm SEM of $n = 3$. (B) Frequency of control (+/+) and *Dnmt3a*-mutant (R878H/+) HSPCs in live, early apoptotic, late apoptotic, or necrotic gates after stimulation with 0, 100, or 500 ng/mL OSM for 24 hours. Bars represent mean \pm SEM of $n = 3$. (C) CFU in control (+/+) and *Dnmt3a*-mutant (R878H/+) HSPCs with 0, 100, or 500 ng/mL OSM. Dots represent individual mice. $n = 5$. (D) Serial CFU in control (+/+) and *Dnmt3a*-mutant (R878H/+) HSPCs (left) and HSCs (right) with 0 or 500 ng/mL OSM. Dots show individual mice, bars represent mean \pm SEM of $n = 3-4$. ** $p < 0.01$; **** $p < 0.0001$ by two-way ANOVA with Tukey's multiple comparisons test. (E) Total viable cells from control (+/+) and *Dnmt3a*-mutant (R878H/+) HSCs, MPP^{G/M}, and GMP after 48 hours of culture with 0 or 500 ng/mL OSM. Dots show individual mice, bars represent mean \pm SEM of $n = 3$. ANOVA=Analysis of variance; CFUs=colony-forming units; HSCs=hematopoietic stem cells; HSPCs=hematopoietic stem and progenitor cells; GMP=granulocyte-macrophage progenitors; MPP^{G/M}=granulocyte/macrophage-primed multipotent progenitors; OSM=Oncostatin M.

OSM was added to previously defined 'cytokine-poor' (SCF, G-CSF) and 'cytokine-rich' (SCF, GM-CSF, IL-3, IL-11, Flt3L, TPO, EPO) media [28] to replicate stress and nonstress conditions, respectively. Control and *Dnmt3a*-mutant HSCs as well as two progenitor populations (MPP^{G/M} and GMPs) were prospectively isolated from young adult mice and cultured in cytokine-poor and cytokine-rich media for 48 hours. After this culture period, total viable cell counts were obtained using flow cytometry. No significant differences in total viable cell counts were observed between genotype and treatment groups for any of the input cell populations (Figure 2E). Together,

these data suggest that young control and young *Dnmt3a*-mutant HSPCs do not respond to acute OSM stimulation through altered cell cycling, apoptosis, myeloid differentiation, or proliferation.

Acute OSM Stimulation Does Not Alter Engraftment Potential or Lineage Output from Young *Dnmt3a*-Mutant HSPCs

As in vitro assays do not fully reflect the in vivo functional potential of HSPCs, we next tested the hypothesis that recombinant OSM as a single stimulus would be sufficient to promote the selective advantage

of young *Dnmt3a*-mutant (R878H/+) HSPCs and HSCs in vivo. First, 50 prospectively isolated HSCs from young adult donor CD45.2+ control or *Dnmt3a*-mutant mice were cultured in conditions designed to promote HSC self-renewal [29] supplemented with 500 ng/mL recombinant murine OSM or vehicle control (Figure 3A). After 7 days of culture, the resulting cells in each well were transplanted into lethally irradiated CD45.1+ recipient mice to assess hematopoietic engraftment and lineage potential. At 16 weeks post-transplant, no significant differences were observed in donor engraftment (% CD45.2+) in the PB or BM of recipient mice (Figure 3B). Analysis of lineage composition of the PB graft revealed an increased proportion of B cells from *Dnmt3a*-mutant versus control vehicle-treated HSCs, as we have previously observed (Figure 3C) [18]. However, no significant differences were observed in PB lineage composition in recipient mice based on acute OSM stimulation. We also did not observe changes in donor-derived BM HSPCs subsets, including HSCs, MPP^{G/M}, CMPs, and GMPs, due to acute OSM stimulation (Figure 3D).

To evaluate the effect of OSM on cellular competition between *Dnmt3a*-mutant and control hematopoiesis, we utilized competitive transplantation. In total, 25 prospectively isolated HSCs from young adult donor CD45.2+ control or *Dnmt3a*-mutant mice were mixed with 25 prospectively isolated HSCs from competitor CD45.2+ CD45.1+ (F1 hybrid) mice. These were cultured in the same conditions as above, supplemented with 500 ng/mL recombinant murine OSM or vehicle control (Figure 3E). After 7 days of culture, the resulting cells in each well were transplanted into lethally irradiated CD45.1+ recipient mice to assess hematopoietic engraftment and lineage potential. At 16 weeks post-transplant, no significant differences in donor engraftment (% CD45.2+) were observed in the PB or BM of recipient mice (Figure 3F). Analysis of lineage composition of the PB graft revealed an increased proportion of B cells from *Dnmt3a*-mutant versus control vehicle-treated HSCs (Figure 3G), consistent with the findings above. However, no significant differences were observed in PB lineage composition in recipient mice based on acute OSM stimulation. In addition, no changes were observed in donor-derived BM HSPCs subsets, including HSCs, MPP^{G/M}, CMPs, and GMPs, due to acute OSM stimulation (Figure 3H). Together, these data suggest that acute OSM stimulation does not lead to changes in engraftment or lineage potential of young *Dnmt3a*-mutant HSPCs in noncompetitive or competitive transplant experiments.

Young *Dnmt3a*-Mutant HSCs are Responsive to Acute OSM Stimulation via STAT3 Phosphorylation and Transcriptional Alterations

Based on a lack of phenotypic alterations associated with recombinant OSM stimulation of young control and young *Dnmt3a*-mutant HSCs in vitro and in vivo, we evaluated the extent to which these cells have the capacity to directly bind and respond to recombinant murine OSM. We first considered antibody-based assessment of levels of the OSM receptor subunit OSMR on the cell surface. Due to a lack of specific and commercially available anti-mouse OSMR antibodies [35], recombinant OSM was fluorescently labeled (OSM-AF488) and used to test binding and labeling of *Dnmt3a*-mutant and control HSCs, in comparison to negative (no OSM-AF488) and positive (liver cells with OSM-AF488) controls. OSM-AF488 was found

to bind both control and R878H/+ HSCs (Supplementary Figure E1A), supporting that control and *Dnmt3a*-mutant HSCs are capable of directly binding recombinant murine OSM.

To test STAT3 activation by recombinant OSM, we prospectively isolated control and *Dnmt3a*-mutant HSPCs from young adult mice, stimulated ex vivo with 500 ng/mL of recombinant murine OSM over a time course, and evaluated phosphorylation of STAT3 and STAT5 by flow cytometry (Figure 4A). Acute OSM stimulation of *Dnmt3a*-mutant HSPCs resulted in greater pSTAT3 compared with vehicle-stimulated *Dnmt3a*-mutant HSPCs as well as OSM-stimulated control HSPCs after 60 min (Figure 4B). No differences were observed in pSTAT3 in any condition after 20 min or 80 min stimulation, indicating tight regulation of the OSM-STAT3 signaling response. No differences in pSTAT5 were observed in any condition at any of the tested time points (Supplementary Figure E1B), demonstrating selectivity of the acute OSM signaling response toward STAT3 activation in young *Dnmt3a*-mutant HSPCs.

We tested the transcriptional consequences of OSM-STAT3 signaling in a more purified control and *Dnmt3a*-mutant HSC population. Control and *Dnmt3a*-mutant HSCs were prospectively isolated from young adult mice, stimulated ex vivo with 500 ng/mL of recombinant murine OSM or vehicle control for 60 min, and immediately flash frozen to prepare cell pellets for RNA extraction and RNA-seq. We identified significantly differentially expressed genes comparing OSM- versus vehicle-treated control HSCs and OSM- versus vehicle-treated *Dnmt3a*-mutant HSCs using $p < 0.05$ and $FC \pm 1.5$ cutoffs. This analysis revealed OSM-treated control HSCs had 385 genes with increased expression and 391 genes with decreased expression (Figure 4C). In contrast, OSM-treated *Dnmt3a*-mutant HSCs had 507 genes with increased expression and 299 genes with decreased expression (Figure 4D). Of the 385 OSM-activated genes in control HSCs and the 507 OSM-activated genes in *Dnmt3a*-mutant HSCs, only 19 were overlapping, suggesting a fundamentally distinct transcriptional response of young *Dnmt3a*-mutant HSCs to acute OSM. Delving further into specific gene alterations, we noted that acute OSM-stimulated *Dnmt3a*-mutant HSCs had robust upregulation of several key inflammatory molecules, receptors, and response factors, including *Il6*, *Il1b*, *Tnf*, *Il1r2*, *Csf3r*, *Ccr1*, and *Irf1*. Apart from *Il1b*, these were not upregulated in OSM-stimulated control HSCs. These data suggests that a 60-min stimulation of young *Dnmt3a*-mutant HSCs with recombinant OSM is sufficient to induce transcriptional upregulation of inflammatory cytokines associated with *Dnmt3a*-mutant CH.

To further interrogate these transcriptional signatures, we performed enrichment analyses using Gene Ontology terms as well as using the molecular signatures database (MSigDB). Acute OSM-stimulated genes in *Dnmt3a*-mutant HSCs were enriched for focused signatures of inflammation, apoptosis, immune defense/stress responses, innate immunity, hematopoiesis, and myeloid cell development (Figure 4F). In contrast, OSM-stimulated genes in control HSCs were enriched for generic signatures of DNA metabolic processes, cell motility and morphogenesis, vesicle-mediated transport, and cell cycle-related processes (Myc/Max targets and E2F4 binding) (Figure 4E). Together, acute stimulation of *Dnmt3a*-mutant HSCs with recombinant OSM results in OSM binding, STAT3 phosphorylation, and transcriptional activation of an inflammatory gene network including the inflammatory cytokines IL-6, TNF α , and IL-1 β that are associated with *Dnmt3a*-mutant CH in mice and humans.

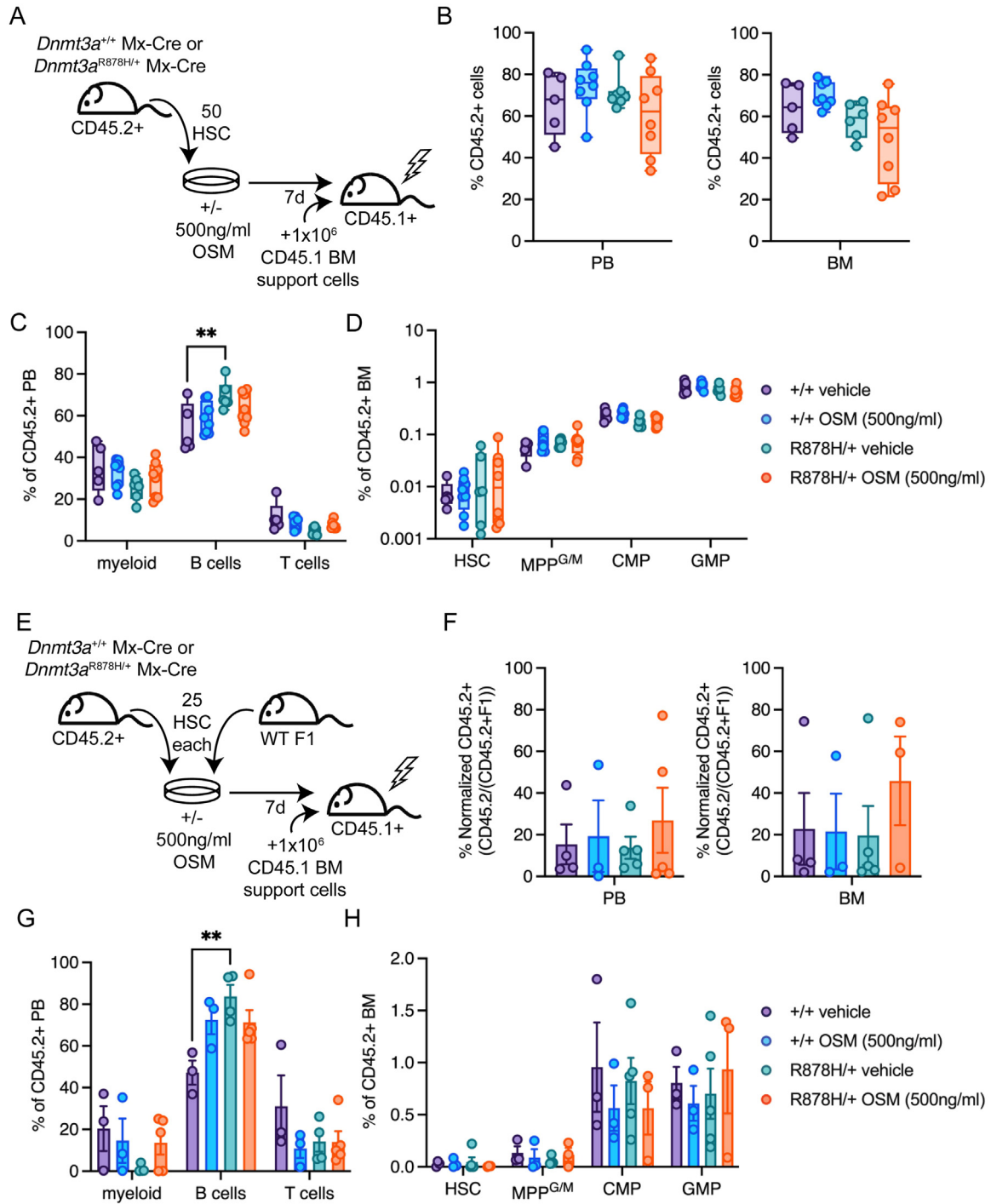


Figure 3 Engraftment potential and lineage output from young *Dnmt3a*-mutant HSPCs is unaltered by acute OSM stimulation. **(A)** Schematic of transplant design. **(B)** Frequency of donor CD45.2⁺ cells in the PB and BM at 16 weeks post-transplant of control (+/+) and *Dnmt3a*-mutant (R878H/+) HSCs treated with 0 or 500 ng/mL OSM for 7 days. **(C)** Donor-derived PB lineage (myeloid, B and T cell) frequencies. **(D)** Donor-derived BM hematopoietic stem and progenitor cell frequencies. **(E)** Schematic of competitive transplant design. **(F)** Normalized frequency of donor CD45.2⁺ cells in PB and BM at 16 weeks post-transplant of control (+/+) and *Dnmt3a*-mutant (R878H/+) HSCs treated with 0 or 500 ng/mL OSM for 7 days. **(G)** Donor-derived PB lineage (myeloid, B and T cell) frequencies. **(H)** Donor-derived BM HSPC frequencies. In all figures, dots show individual mice and bars represent mean ± SEM of *n* = 3–8. ***p* < 0.01 by two-way ANOVA with Tukey's multiple comparisons test. ANOVA=Analysis of variance; BM=bone marrow; HSPCs=hematopoietic stem and progenitor cells; OSM=Oncostatin M; PB=peripheral blood.

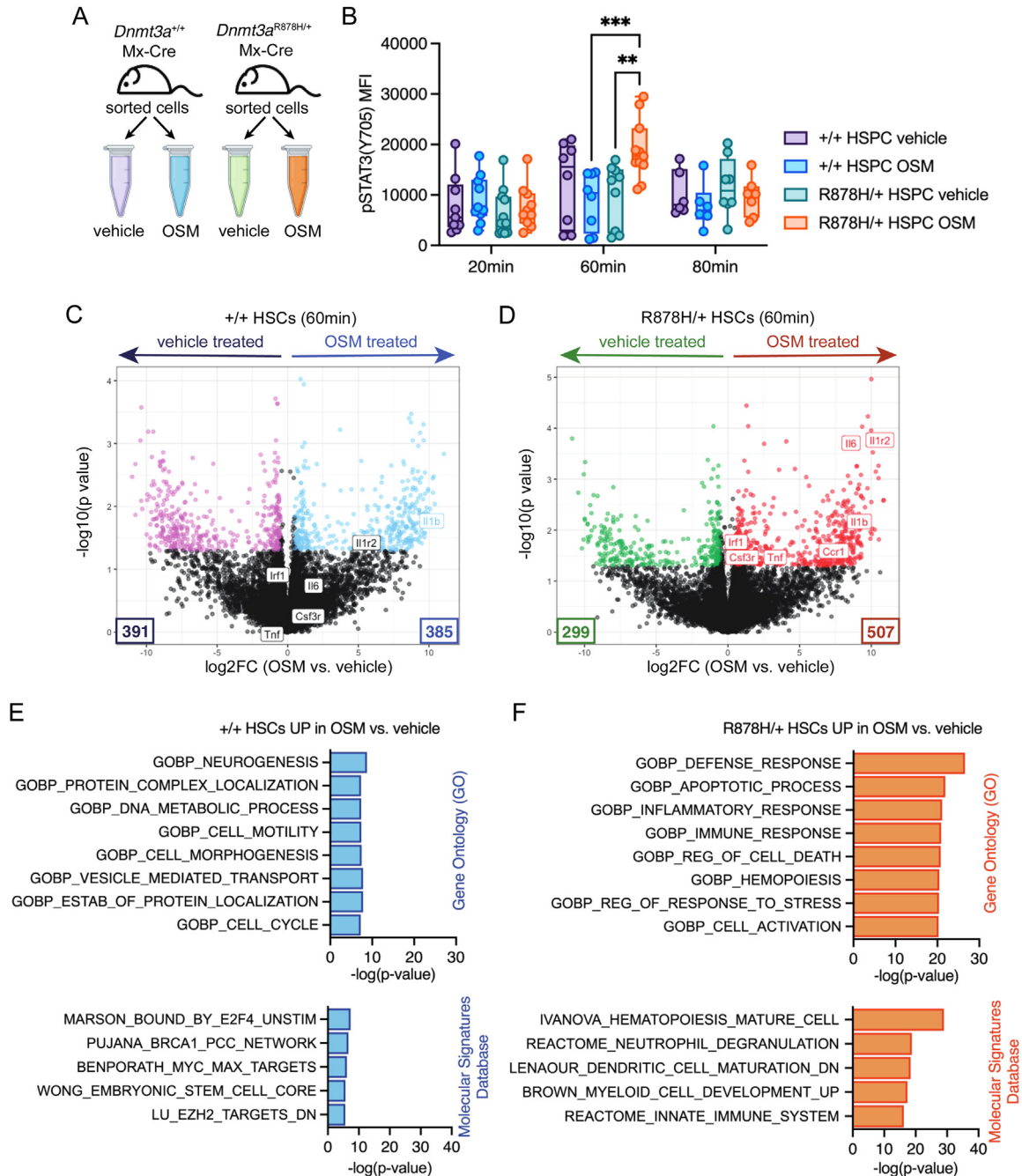


Figure 4 Acute OSM stimulation activates STAT3 phosphorylation and transcriptional responses in young *Dnmt3a*-mutant HSCs. **(A)** Schematic of experimental design. **(B)** MFI of pSTAT3 (Y705) in control (+/+) and *Dnmt3a*-mutant (R878H/+) HSPCs treated with 0 or 500 ng/mL OSM for 20, 60, and 80 min. Dots show individual mice and bars represent mean \pm SEM of $n = 6-10$. ** $p < 0.01$; *** $p < 0.001$ by mixed-effects analysis with Tukey's multiple comparisons test. **(C, D)** Volcano plot showing differential gene expression of **(C)** control (+/+) and **(D)** *Dnmt3a*-mutant (R878H/+) HSCs treated with 0 or 500 ng/mL OSM for 60 min. $n = 6$ biological replicates. Select genes involved in STAT3 signaling and inflammation are labeled. **(E, F)** Enrichment analysis of significantly differentially expressed genes in **(E)** control (+/+) and **(F)** *Dnmt3a*-mutant (R878H/+) HSCs treated with 500 ng/mL vs. 0 ng/mL OSM for 60 min. HSCs=Hematopoietic stem cells; HSPCs=hematopoietic stem and progenitor cells; MFI=mean fluorescence intensity; OSM=Oncostatin M.

Young *Dnmt3a*-Mutant HSCs Upregulate Anti-Inflammatory Genes and Stabilize *Socs3* in Response to Acute OSM Stimulation

We sought to resolve the disconnect we observed between acute OSM-driven STAT3 signaling and transcriptional activation in *Dnmt3a*-mutant (R878H/+) HSCs and the lack of phenotypic changes in *Dnmt3a*-mutant HSCs and HSPCs. Previous studies have found elevated expression of suppressors of inflammation, such as *Socs3*, *Nr4a1*, and *Atf3*, in CH-mutant HSPCs [36], and OSM has been reported to stimulate expression of *Socs3* in other cell types [37,38]. Thus, we hypothesized that acute OSM stimulation of young *Dnmt3a*-mutant HSCs results in enhanced expression of suppressors of inflammation. Interrogating our OSM- versus vehicle-treated *Dnmt3a*-mutant HSC RNA-seq data revealed that *Socs3*, *Nr4a1*, and *Atf3* were increased in expression after acute OSM stimulation (Figure 5A).

To evaluate the dynamics of transcript induction, we focused on *Socs3*. Control and R878H/+ HSPCs were prospectively isolated from young adult mice and stimulated with 0 or 500 ng/mL recombinant murine OSM for up to 80 min. Cells were flash-frozen for RNA extraction, cDNA synthesis and quantitative real-time PCR for *Socs3*. OSM stimulation of control HSPCs resulted in a small, but significant, increase in *Socs3* after 60 min (Figure 5B). In contrast, OSM stimulation of *Dnmt3a*-mutant HSPCs resulted in robust increase in *Socs3* at 20, 40, and 60 min. This result demonstrates that *Dnmt3a*-mutant HSPCs rapidly respond to OSM stimulation by upregulating *Socs3* at both greater levels and a faster rate compared with control HSPCs.

To evaluate stability of the *Socs3* mRNA transcript, we prospectively isolated control and *Dnmt3a*-mutant HSPCs from young adult mice and stimulated with 0 or 500 ng/mL recombinant murine OSM for 60 min, a timepoint we have consistently shown to result in STAT3 phosphorylation and transcriptional responses in *Dnmt3a*-mutant HSPCs. OSM stimulation was followed by the incubation of cells for 0, 20, 60, and 80 min with actinomycin D, to pause transcription and allow the study of transcript stability over time [39]. Cells were flash-frozen for RNA extraction, cDNA synthesis and real-time PCR for *Socs3*. Consistent with the above results, *Socs3* was robustly increased in *Dnmt3a*-mutant HSPCs at 60 min of OSM stimulation (Figure 5C). Furthermore, OSM-stimulated *Dnmt3a*-mutant HSPCs maintained increased levels of *Socs3* for up to 80 min of actinomycin D treatment. These results suggest that OSM-stimulated *Dnmt3a*-mutant HSPCs have a robust increase in *Socs3* transcript expression. In addition, this transcript is stably maintained for up to 140 min following exposure to OSM. We posit that *Socs3* activation may suppress STAT3 signaling, silencing transcriptional responses to OSM before functional outcomes are realized.

Dnmt3a-mutant HSCs Do Not Upregulate Anti-Inflammatory Genes in the Context of an Aged Environment

At the beginning of our study, we discovered a transcriptional program of inflammation response in *Dnmt3a*-mutant compared with control HSCs in middle-aged, but not young, transplant recipient mice (Figure 1B). Thus, we hypothesized that middle-aged mice have elevated 'chronic' levels of OSM and that *Dnmt3a*-mutant HSCs in a middle-aged microenvironment lose the capacity to upregulate suppressors of inflammation such as *Socs3*, *Nr4a1*, and *Atf3*. BM fluid was collected from young adult (3 months), middle-aged (14

months), and old (22 months) wild-type C57BL/6 mice, and OSM abundance was quantified using ELISA. A significant and progressive increase in the quantity of OSM in the BM fluid was observed from young to middle-aged to old mice (Figure 6A). We examined our published RNA-seq data of control and *Dnmt3a*-mutant HSCs re-isolated from transplanted middle-aged wild-type recipient mice, focusing on the key inflammatory molecules identified in our acute OSM-stimulated *Dnmt3a*-mutant HSCs (Figure 4D) as well as *Socs3*, *Nr4a1*, and *Atf3*. *Dnmt3a*-mutant HSCs compared with control HSCs in transplanted middle-aged recipient mice had robust upregulation of *Il1r2*, *Il1b*, *Ccr1*, *Tnf*, and *Csf3r* (Figure 6B). Unlike acute OSM-stimulated *Dnmt3a*-mutant HSCs, we did not observe increased expression of *Socs3*, *Nr4a1*, or *Atf3*.

DISCUSSION

We report a role for Oncostatin M (OSM) in transcriptional induction of a cytokine network in *Dnmt3a*-mutant CH. Our initial discovery was based on transcriptional signatures indicating active OSM signaling in *Dnmt3a*-mutant HSCs specifically in the context of a middle-aged BM microenvironment. In functional experiments, OSM stimulation of young *Dnmt3a*-mutant HSCs did not impact hematopoietic cell function or output in vitro or in vivo; however, it did result in STAT3 phosphorylation and a transcriptional inflammatory response including upregulation of *Il6*, *Il1b*, and *Tnf*. Focused studies of transcript production and stability revealed a putative negative feedback mechanism in young *Dnmt3a*-mutant HSCs where OSM signaling results in increased transcription and transcript stability of anti-inflammatory genes, including *Socs3*, *Nr4a1*, and *Atf3*. In the context of a middle-aged BM microenvironment, *Dnmt3a*-mutant HSCs upregulate inflammation-related transcripts, but this response is not accompanied by upregulation of anti-inflammatory genes. Of note, the levels of OSM in our ex vivo versus in vivo studies are distinct; thus, we are unable to draw direct conclusions about OSM-responsive genes in the middle-aged microenvironment context. We hypothesize that chronic inflammation with aging, be it through OSM or mediated by other cytokines, may exhaust the regulatory mechanisms present in young *Dnmt3a*-mutant HSCs that resolve inflammatory states (Figure 6C).

OSM is an IL-6 family cytokine known to be involved in the immunopathogenesis of colon cancer, breast cancer, pancreatic cancer, myeloma, and hepatoblastoma [35]. Whereas IL-6 represents one of the most studied cytokines to date, the physiological activities of OSM are less well known. OSM is predominantly produced by T lymphocytes, macrophages, and neutrophils [19] and signals through the heterodimeric receptor gp130/OSMR in mice [40]. OSM is a strong inducer of JAK/STAT signaling, leading to activation of STAT3 and STAT5 [41,42]. OSM is an important regulator of the BM microenvironment in both steady state and in regeneration after injury [43,44] with endothelial and mesenchymal cells being major cell types expressing OSMR [35]. In addition, OSM plays a role in HSC mobilization via its effects on nonhematopoietic cells in the BM microenvironment [35]. These data and models support a role for OSM as a cytokine produced by mature hematopoietic cells that impacts the functionality of nonhematopoietic cells in the BM microenvironment. Previous studies performed in young adult mice have shown that *Osmr* is not detected in HSPCs or myeloid cells [35]; thus, it has been suggested that HSCs and their progeny do not

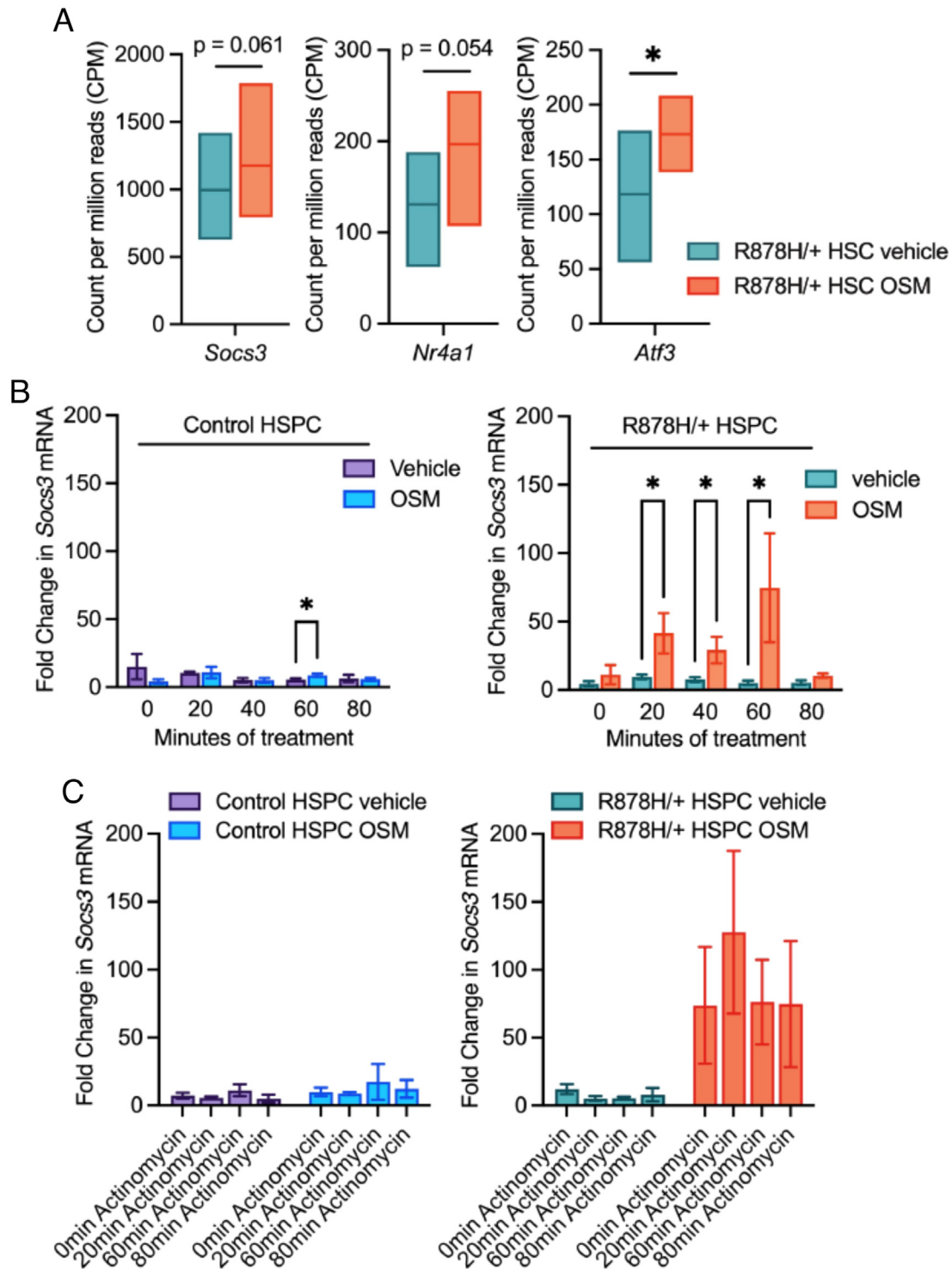


Figure 5 *Dnmt3a*-mutant HSCs exhibit upregulation of *Soxs3*, *Nr4a1*, and *Atf3* in response to acute recombinant OSM stimulation. **(A)** *Soxs3*, *Nr4a1*, and *Atf3* expression in control (+/) and *Dnmt3a*-mutant (R878H/+) HSCs stimulated with 0 or 500 ng/mL OSM for 60 min. Box plots summarize $n = 6$ replicates per condition. $*p < 0.05$. **(B)** *Soxs3* expression in control (+/) and *Dnmt3a*-mutant (R878H/+) HSPCs stimulated with 0 or 500 ng/mL OSM for described amount of time. Bars represent mean \pm SEM of $n = 3$ –4 replicates. $*p < 0.05$ by multiple-ratio, paired sample t test. **(C)** *Soxs3* expression in control (+/) and *Dnmt3a*-mutant (R878H/+) HSPCs stimulated with 0 or 500 ng/mL of OSM for 60 min followed by actinomycin D for 0, 20, 60, and 80 min. Bars represent mean \pm SEM of $n = 4$ replicates. HSCs=Hematopoietic stem cells; HSPCs=hematopoietic stem and progenitor cells; OSM=Oncostatin M.

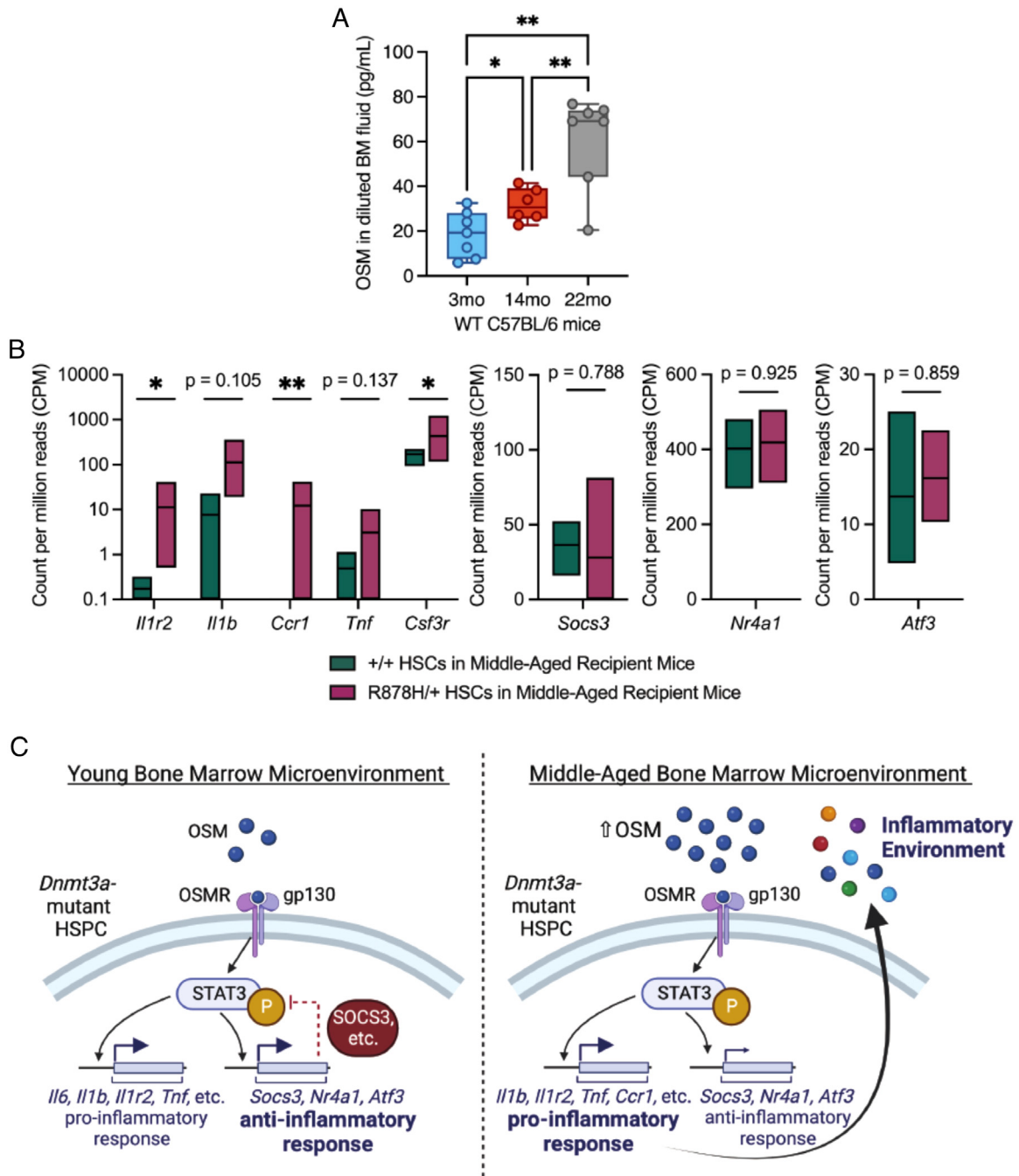


Figure 6 *Dnmt3a*-mutant HSCs do not differentially express *Socs3*, *Nr4a1*, and *Atf3* in a middle-aged BM microenvironment. **(A)** OSM concentration in bone marrow fluid in young (3 month), middle-aged (14 month) and old (22mo) wild-type C57BL/6 mice. Dots show individual mice; bars represent mean \pm SEM of $n = 6-7$. $*p < 0.05$; $**p < 0.01$ by Brown-Forsythe and Welch's ANOVA with multiple comparisons. **(B)** Expression of inflammatory genes *Il1r2*, *Il1b*, *Ccr1*, *Tnf*, and *Csf3r*, and the anti-inflammatory genes *Socs3*, *Nr4a1*, and *Atf3* in control (+/+) and *Dnmt3a*-mutant (R878H/+) HSCs after 4 months post-transplant in middle-aged recipient mice. Box plots summarize $n = 3-4$ replicates per condition. $*p < 0.05$; $**p < 0.01$ by multiple-ratio, paired sample t test. **(C)** Working model of OSM signaling in *Dnmt3a*-mutant HSPCs in the context of the young and middle-aged BM environments. Created with BioRender.com licensed by The Jackson Laboratory. ANOVA=Analysis of variance; BM=bone marrow; HSCs=hematopoietic stem cells; HSPCs=hematopoietic stem and progenitor cells; OSM=Oncostatin M.

directly respond to OSM. However, *Osmr* is one of the most upregulated transcripts in old HSCs compared with young HSCs across six independent datasets [45], suggesting that in certain contexts, such as aging, HSCs and their progeny gain the capacity to respond to OSM. Our data show that HSCs, in the context of a CH-relevant mutation in *Dnmt3a*, have the capacity to phosphorylate STAT3 and undergo transcriptional alterations in response to recombinant OSM. The extent to which this transcriptional response is physiologically relevant with respect to cellular function is an important question that should be addressed in future studies focused on the aged BM microenvironment.

Previous literature has demonstrated that OSM leads to a stronger and prolonged induction of *SOCS3* compared with IL-6 stimulation in HepG2 cells and mouse embryonic fibroblasts [38]. Our observations suggest that stimulation with recombinant OSM at high concentrations results in transcriptional upregulation of the cytokine family member *Il6* in addition to *Socs3*. Given that IL-6 is also a potent inducer of *Socs3* and has been identified as a key inflammatory signal in the fatty BM that drives *DNMT3A*-mutant CH in human and mouse models, it remains a possibility that both OSM and IL-6 contribute to induction and stability of the *Socs3* transcript. Recently, Potts et al. reported that splicing factor (*Sf3b1*) mutant HSPCs had similar STAT3 phosphorylation following stimulation with OSM and IL-6 together compared with OSM alone [46], although they did not directly evaluate *Socs3*. In a thought-provoking study, *Socs3* was found to serve an essential role in maintaining specificity of STAT3 phosphorylation and gene transcription in response to IL-6 versus G-CSF, supporting that STAT3 signaling is uniquely regulated in a cytokine-dependent manner [47]. Distinctions between *Socs3* induction and stability driven by OSM versus other STAT3 signaling inducers will be interesting to explore in future studies.

The consequences of OSM signaling have been found to be context-dependent, resulting in proinflammatory as well as anti-inflammatory/anti-proliferative outcomes [41]. This is consistent with our data in young *Dnmt3a*-mutant HSCs where both proinflammatory cytokines as well as anti-inflammatory molecules are expressed in response to OSM. This anti-inflammatory negative feedback loop may be a conserved mechanism facilitating the selective advantage of mutant HSCs in CH. Recent work using a zebrafish model of human *ASXL1*-mutant CH found a protective response to proinflammatory cytokines in HSPCs via upregulation of *socs3a*, *atf3*, and *nr4a1* [36]. Without the capacity to upregulate *nr4a1* and *nr4a3*, *Asxl1*-mutant HSPCs lost their self-renewal capacity and selective growth advantage. In addition to induction of these anti-inflammatory transcripts that work in part through silencing STAT3 activation, complementary mechanisms may allow mutant HSCs to survive in a chronic inflammatory environment associated with aging. For example, in *Tet2*-mutant CH, HSPCs with hyperactivated SHP2-STAT3 signaling downregulate the apoptotic protein Bim via the anti-apoptotic long noncoding RNA *Morbid* [38]. Together, complexities in the regulation of and response to inflammation in various forms of CH prompts careful consideration of effective targeting strategies to ameliorate CH-associated disease states in the context of aging.

Conflict of Interest Disclosure

J.J.T. has received research support from H3 Biomedicine, Inc., and patent royalties from Fate Therapeutics. All other authors declare no competing interests.

Acknowledgements

This work was supported by National Institutes of Health (Bethesda, MD, USA) Grants [R01DK118072](#), [R01AG069010](#), and [U01AG077925](#) and a grant from the Edward P. Evans Foundation (Andover, MA, USA) to J.J.T. This work was supported in part by the National Cancer Institute (Bethesda, MD, USA) Cancer Center Support Grant [P30CA034196](#). J.J.T. was supported by a Leukemia & Lymphoma Society (Rye Brook, NY, USA) Scholar Award and The Dattels Family Endowed Chair. L.S.S. was supported by National Institutes of Health (Bethesda, MD, USA) [F31DK127573](#) and The Tufts University Scheer-Tomasso Fund philanthropic gift. We thank all members of the Trowbridge Lab for experimental support and manuscript editing. We thank the Scientific Services at The Jackson Laboratory, including flow cytometry and genome technologies. We thank Drs. Carol Bult, Ryan Tewhey, Cliff Rosen, and Phil Hinds for their critical input into this work.

Author Contributions

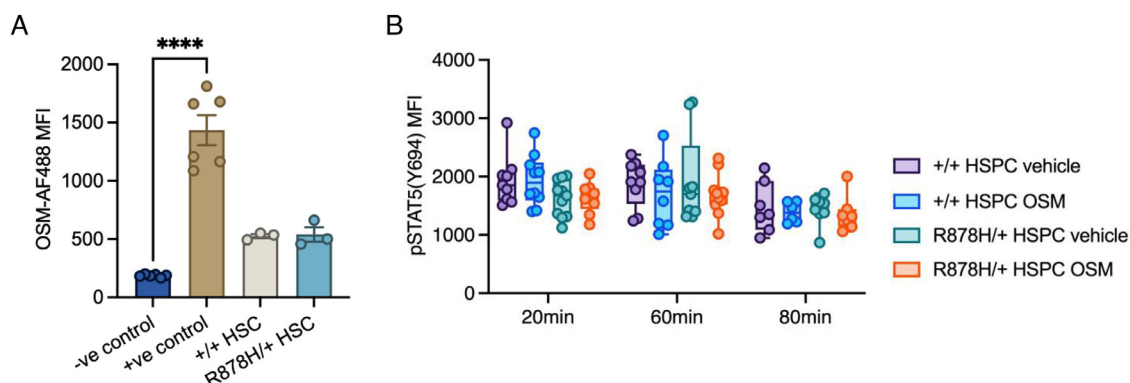
L.S.S. and J.J.T. conceptualized the project and designed experiments. L.S.S. performed experiments and analyzed data with assistance from K.A.Y., N.B., and K.D.M. RNA-seq data were analyzed and graphed by L.S.S. and T.M.S. The manuscript was written by L.S.S. and J.J.T. All authors edited the manuscript.

REFERENCES

- Jaiswal S, Fontanillas P, Flannick J, et al. Age-related clonal hematopoiesis associated with adverse outcomes. *N Engl J Med* 2014;371:2488–98.
- Genovese G, Kahler AK, Handsaker RE, et al. Clonal hematopoiesis and blood-cancer risk inferred from blood DNA sequence. *N Engl J Med* 2014;371:2477–87.
- Colom Diaz PA, Mistry JJ, Trowbridge JJ. Hematopoietic Stem Cell Aging and Leukemia Transformation. *Blood* 2023;142:533–42.
- Bhattacharya R, Zekavat SM, Haessler J, et al. Clonal hematopoiesis is associated with higher risk of stroke. *Stroke* 2022;53:788–97.
- Mooney L, Goodyear CS, Chandra T, et al. Clonal haematopoiesis of indeterminate potential: intersections between inflammation, vascular disease and heart failure. *Clin Sci (Lond)* 2021;135:991–1007.
- Papaemmanuil E, Gerstung M, Malcovati L, et al. Clinical and biological implications of driver mutations in myelodysplastic syndromes. *Blood* 2013;122:3616–27.
- Xie M, Lu C, Wang J, et al. Age-related mutations associated with clonal hematopoietic expansion and malignancies. *Nat Med* 2014;20:1472–8.
- Busque L, Patel JP, Figueroa ME, et al. Recurrent somatic TET2 mutations in normal elderly individuals with clonal hematopoiesis. *Nat Genet* 2012;44:1179–81.
- Nagase R, Inoue D, Pastore A, et al. Expression of mutant *Asxl1* perturbs hematopoiesis and promotes susceptibility to leukemic transformation. *J Exp Med* 2018;215:1729–47.
- Jaiswal S, Libby P. Clonal haematopoiesis: connecting ageing and inflammation in cardiovascular disease. *Nat Rev Cardiol* 2020;17:137–44.
- Nachun D, Lu AT, Bick AG, et al. Clonal hematopoiesis associated with epigenetic aging and clinical outcomes. *Aging Cell* 2021;20:e13366.
- SanMiguel JM, Young K, Trowbridge JJ. Hand in hand: intrinsic and extrinsic drivers of aging and clonal hematopoiesis. *Exp Hematol* 2020;91:1–9.
- Trowbridge JJ, Starczynowski DT. Innate immune pathways and inflammation in hematopoietic aging, clonal hematopoiesis, and MDS. *J Exp Med* 2021;218:e20201544.
- Florez MA, Tran BT, Wathan TK, et al. Clonal hematopoiesis: mutation-specific adaptation to environmental change. *Cell Stem Cell* 2022;29:882–904.

15. Zhang CRC, Nix D, Gregory M, et al. Inflammatory cytokines promote clonal hematopoiesis with specific mutations in ulcerative colitis patients. *Exp Hematol* 2019;80:36–41.e3.
16. Hormaechea-Agulla D, Matatall KA, Le DT, et al. Chronic infection drives Dnmt3a-loss-of-function clonal hematopoiesis via IFN γ signaling. *Cell Stem Cell* 2021;28:1428–1442.e6.
17. Zioni N, Bercovich AA, Chapal-Ilani N, et al. Inflammatory signals from fatty bone marrow support DNMT3A driven clonal hematopoiesis. *Nat Commun* 2023;14:2070.
18. SanMiguel JM, Eudy E, Loberg MA, et al. Distinct tumor necrosis factor alpha receptors dictate stem cell fitness versus lineage output in Dnmt3a-mutant clonal hematopoiesis. *Cancer Discov* 2022;12:2763–73.
19. Cai Z, Kotzin JJ, Ramdas B, et al. Inhibition of inflammatory signaling in Tet2 mutant preleukemic cells mitigates stress-induced abnormalities and clonal hematopoiesis. *Cell Stem Cell* 2018;23:833–849.e5.
20. Cook EK, Izukawa T, Young S, et al. Comorbid and inflammatory characteristics of genetic subtypes of clonal hematopoiesis. *Blood Adv* 2019;3:2482–6.
21. Caiado F, Kovtonyuk LV, Gonullu NG, Fullin J, Boettcher S, Manz MG. Aging drives Tet2 $^{+/-}$ clonal hematopoiesis via IL-1 signaling. *Blood* 2023;141:886–903.
22. Fuster JJ, Zuriaga MA, Zorita V, et al. TET2-loss-of-function-driven clonal hematopoiesis exacerbates experimental insulin resistance in aging and obesity. *Cell Rep* 2020;33:108326.
23. Bick AG, Weinstock JS, Nandakumar SK, et al. Inherited causes of clonal haematopoiesis in 97,691 whole genomes. *Nature* 2020;586:763–8.
24. Abegunde SO, Buckstein R, Wells RA, et al. An inflammatory environment containing TNF α favors Tet2-mutant clonal hematopoiesis. *Exp Hematol* 2018;59:60–5.
25. Fujino T, Goyama S, Sugiura Y, et al. Mutant ASXL1 induces age-related expansion of phenotypic hematopoietic stem cells through activation of Akt/mTOR pathway. *Nat Commun* 2021;12:1826.
26. Loberg MA, Bell RK, Goodwin LO, et al. Sequentially inducible mouse models reveal that Npm1 mutation causes malignant transformation of Dnmt3a-mutant clonal hematopoiesis. *Leukemia* 2019;33:1635–49.
27. Shen FW, Saga Y, Litman G, et al. Cloning of Ly-5 cDNA. *Proc Natl Acad Sci U S A* 1985;82:7360–3.
28. Yamashita M, Passegue E. TNF-alpha coordinates hematopoietic stem cell survival and myeloid regeneration. *Cell Stem Cell* 2019;25:357–372.e7.
29. Wilkinson AC, Ishida R, Kikuchi M, et al. Long-term ex vivo haematopoietic-stem-cell expansion allows nonconditioned transplantation. *Nature* 2019;571:117–21.
30. Tawara K, Scott H, Emathinger J, et al. HIGH expression of OSM and IL-6 are associated with decreased breast cancer survival: synergistic induction of IL-6 secretion by OSM and IL-1 β . *Oncotarget* 2019;10:2068–85.
31. Chauhan D, Kharbanda SM, Ogata A, et al. Oncostatin M induces association of Grb2 with Janus kinase JAK2 in multiple myeloma cells. *J Exp Med* 1995;182:1801–6.
32. Chen M, Ren R, Lin W, Xiang L, Zhao Z, Shao B. Exploring the oncostatin M (OSM) feed-forward signaling of glioblastoma via STAT3 in pancreatic analysis. *Cancer Cell Int* 2021;21:565.
33. Lee BY, Hogg EKJ, Below CR, et al. Heterocellular OSM-OSMR signaling reprograms fibroblasts to promote pancreatic cancer growth and metastasis. *Nat Commun* 2021;12:7336.
34. Gu ZJ, Costes V, Lu ZY, et al. Interleukin-10 is a growth factor for human myeloma cells by induction of an oncostatin M autocrine loop. *Blood* 1996;88:3972–86.
35. Bisht K, McGirr C, Lee SY, et al. Oncostatin M regulates hematopoietic stem cell (HSC) niches in the bone marrow to restrict HSC mobilization. *Leukemia* 2022;36:333–47.
36. Avagyan S, Henninger JE, Mannherz WP, et al. Resistance to inflammation underlies enhanced fitness in clonal hematopoiesis. *Science* 2021;374:768–72.
37. Ehrling C, Bohmer O, Hahnel MJ, et al. Oncostatin M regulates SOCS3 mRNA stability via the MEK-ERK1/2-pathway independent of p38 (MAPK)/MK2. *Cell Signal* 2015;27:555–67.
38. Stross C, Radtke S, Clahsen T, et al. Oncostatin M receptor-mediated signal transduction is negatively regulated by SOCS3 through a receptor tyrosine-independent mechanism. *J Biol Chem* 2006;281:8458–68.
39. Ratnadiwakara M, Anko ML. mRNA stability assay using transcription inhibition by actinomycin D in mouse pluripotent stem cells. *Bio Protoc* 2018;8:e3072.
40. Adrian-Segarra JM, Schindler N, Gajawada P, et al. The AB loop and D-helix in binding site III of human oncostatin M (OSM) are required for OSM receptor activation. *J Biol Chem* 2018;293:7017–29.
41. Masjedi A, Hajizadeh F, Beigi Dargani F, et al. Oncostatin M: a mysterious cytokine in cancers. *Int Immunopharmacol* 2021;90:107158.
42. Hintzen C, Evers C, Lippok BE, et al. Box 2 region of the oncostatin M receptor determines specificity for recruitment of Janus kinases and STAT5 activation. *J Biol Chem* 2008;283:19465–77.
43. Mukoyama Y, Hara T, Xu M, et al. In vitro expansion of murine multipotential hematopoietic progenitors from the embryonic aorta-gonad-mesonephros region. *Immunity* 1998;8:105–14.
44. Mahony CB, Pasche C, Bertrand JY. Oncostatin M and Kit-ligand control hematopoietic stem cell fate during zebrafish embryogenesis. *Stem Cell Rep* 2018;10:1920–34.
45. Flohr Svendsen A, Yang D, Kim K, et al. A comprehensive transcriptome signature of murine hematopoietic stem cell aging. *Blood* 2021;138:439–51.
46. Potts KS, Cameron RC, Metidji A, et al. Splicing factor deficits render hematopoietic stem and progenitor cells sensitive to STAT3 inhibition. *Cell Rep* 2022;41:111825.
47. Croker BA, Mielke LA, Wormald S, et al. Socs3 maintains the specificity of biological responses to cytokine signals during granulocyte and macrophage differentiation. *Exp Hematol* 2008;36:786–98.

SUPPLEMENTARY MATERIALS



Supplementary Figure E1 Binding of OSM to control and *Dnmt3a*-mutant HSPCs and induction of pSTAT5. **(A)** MFI of fluorescently labeled OSM (OSM-AF488) in negative control (no OSM), positive control (liver), control (+/+), and *Dnmt3a*-mutant (R878H/+) HSCs. Dots show individual mice; bars represent mean \pm SEM of $n = 3-6$. **** $p < 0.0001$ by one-way ANOVA with Dunnett's T3 multiple comparisons test. **(B)** MFI of pSTAT5 (Y694) in control (+/+) and *Dnmt3a*-mutant (R878H/+) HSPCs treated with 0 or 500 ng/mL OSM for 20, 60, and 80 min. Dots show individual mice, and bars represent mean \pm SEM of $n = 6-10$. ** $p < 0.01$; *** $p < 0.001$ by mixed-effects analysis with Tukey's multiple comparisons test. ANOVA=Analysis of variance; HSCs=hematopoietic stem cells; HSPCs=hematopoietic stem and progenitor cells; MFI=mean fluorescence intensity; OSM=Oncostatin M.